

Flip Initial Features: Generalization of Neural Networks for Semi-supervised Node Classification

Yoonhyuk Choi¹, Jiho Choi¹, Taewook Ko¹, Chong-Kwon Kim²
 Seoul National University¹, Korea Institute of Energy Technology²
 Seoul¹, Naju², Republic of Korea
 younhyuk95,jihochoi,taewook.ko@snu.ac.kr
 ckim@kentech.ac.kr

ABSTRACT

Graph neural networks (GNNs) have been widely used under semi-supervised settings. Prior studies have mainly focused on finding appropriate graph filters (e.g., aggregation schemes) to generalize well for both homophilic and heterophilic graphs. Even though these approaches are essential and effective, they still suffer from the sparsity in initial node features inherent in the bag-of-words representation. Common in semi-supervised learning where the training samples often fail to cover the entire dimensions of graph filters (hyperplanes), this can precipitate over-fitting of specific dimensions in the first projection matrix. To deal with this problem, we suggest a simple and novel strategy; create additional space by flipping the initial features and hyperplane simultaneously. Training in both the original and in the flip space can provide precise updates of learnable parameters. To the best of our knowledge, this is the first attempt that effectively moderates the overfitting problem in GNN. Extensive experiments on real-world datasets demonstrate that the proposed technique improves the node classification accuracy up to 40.2 %.

CCS CONCEPTS

• **Computing methodologies** → **Machine learning**.

KEYWORDS

Graph neural networks, Semi-supervised learning, Flipping initial features

ACM Reference Format:

Yoonhyuk Choi¹, Jiho Choi¹, Taewook Ko¹, Chong-Kwon Kim². 2022. Flip Initial Features: Generalization of Neural Networks for Semi-supervised Node Classification. In *Proceedings of ACM Conference (Conference'17)*. ACM, New York, NY, USA, 12 pages. <https://doi.org/10.1145/>

1 INTRODUCTION

With the flux of graphical data, graph neural networks (GNNs) accomplished prominent improvement in various fields including molecular [14] and social networks [11]. Integrating node features and network structures concurrently, they have shown the powerful

Permission to make digital or hard copies of all or part of this work for personal or classroom use is granted without fee provided that copies are not made or distributed for profit or commercial advantage and that copies bear this notice and the full citation on the first page. Copyrights for components of this work owned by others than ACM must be honored. Abstracting with credit is permitted. To copy otherwise, or republish, to post on servers or to redistribute to lists, requires prior specific permission and/or a fee. Request permissions from permissions@acm.org.

Conference'17, July 2017, Washington, DC, USA

© 2022 Association for Computing Machinery.

ACM ISBN 978-1-4503-9236-5/22/10...\$15.00

<https://doi.org/10.1145/>

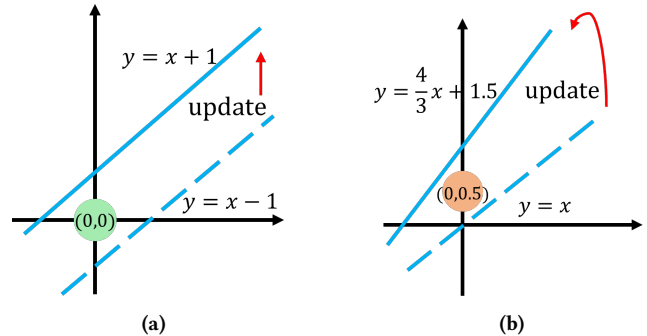


Figure 1: Examples of gradient update using different types of input features; (a) all elements are 0, (b) an element is non-zero. Only the dimension of non-zero value (right) changes the slope of a line

ability for node and graph classification tasks [9, 18, 25, 41]. Message passing, which aggregates features from neighboring nodes recursively, is a key mechanism of GNNs [15].

Recently, many studies have focused on the amelioration of an aggregation scheme to deal with heterogeneous (disassortative) edges [33]. Generally, GNNs fully enjoy the advantage of message passing in homophilic graphs [32]. But in heterogeneous graphs, they struggle to find homophilic neighbors to secure robustness. Several algorithms assign different weights to edges before aggregation [1, 23, 41, 48] or even eliminate disassortative edges [31, 49]. Others further utilize distant nodes with high similarity [21, 34] or adopt node specific propagation using trainable boundaries [44]. We fully understand that the proper selection of aggregation schemes is essential. Nonetheless, we raise another question: *are there other aspects or design spaces beyond aggregation schemes?*

Contrary to previous approaches, we concentrate on the training mechanism of weight matrices (hyperplanes). Our quest originates from an observation that if initial features contain a few non-zero elements (e.g., bag-of-words), insufficiency in training samples (semi-supervised settings) causes overfitting of specific dimensions in the first layer parameters. Figure 1 is a simple example that reveals that a zero feature vector fails to update the slope of a line. While a green node (0, 0) only updates the bias term (please refer to Appendix A for details), an orange node (0, 0.5) in Figure 1b changes slope and bias. Both initial features well classify nodes in this two dimension example, but if the dimensionality is large, the first hyperplane might be biased in certain dimensions. We emphasize that this can

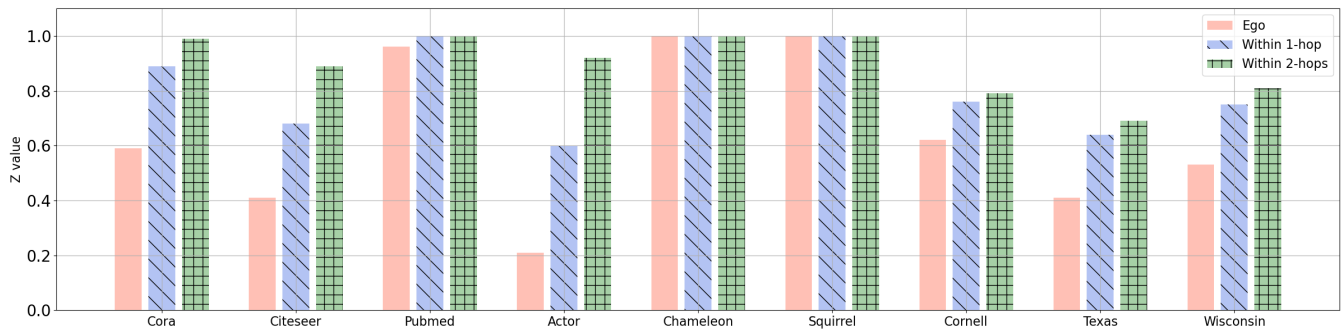


Figure 2: Initial feature distribution of each graph dataset. The definition of z-value is described in Equation 1

harm the quality of predicting test nodes that contain untrained dimensional features.

To better optimize the feature transformation matrix, we focus on the perturbation of the initial features. Our initial choice was a data augmentation mechanism like dimensional image shifting used in computer vision [38]. However, we concluded that shifting is not applicable to GNNs with bag-of-words features where a bit position itself has a specific meaning; positional shifting disarranges the semantic information. Also, compared to the convolutional neural network which ensures local invariance [50], GNNs employ multi-layer perceptron (MLP) which is not translation invariant. We also considered to add a noise [16, 52] to inputs. But, this requires an additional decoding process with a precise selection of hyperparameters and also implicates a normalization problem [4].

We devise a solution that flips the initial features and parameters simultaneously. The proposed flipping scheme is inspired by previous techniques of shifting parameters [24] and rotation of neural networks [29] which can preserve the volume of gradients and initial features. We also focus on a dual path network [7] that a slight change of parameter can ensure our model operates in the original and flipped spaces concurrently. Our method solves the zero gradient problem caused by input data [20] and also facilitates accurate semantic learning of each dimension [30]. The flipping mechanism is orthogonal to GNNs and we apply the flipping mechanism to three representative methods (MLP, GCN, and GAT). We compare the performances of the three variants with state-of-the-art baselines on nine real-world datasets. We observe that the average gain of the three flipping methods, Flip-MLP, Flip-GCN, and Flip-GAT over their originals are 17.2 %, 24.2 %, and 17.8 %, respectively. The contributions of this paper can be summarized as follows:

- We show that GNNs are quite sensitive to initial features and their performance can be largely improved if zero elements are eliminated.
- To solve the problem, we propose a flipping mechanism that concurrently transposes initial features and hyperplane. Unlike previous methods that focus on aggregation schemes, our method scrutinizes the backpropagation and subsidizes precise component-wise guiding of the first hyperplane.
- The proposed flipping mechanism is orthogonal to GNNs. Applying flipping to MLP, GCN, and GAT. we develop three flipping variants. We conduct extensive experiments using

real-world benchmark graphs. The flipping variants surpass all state-of-the-art baselines.

2 PRELIMINARIES

This section starts with the feature distribution of each benchmark dataset. Then, we define the widely used notations of the graph-structured dataset that will be used throughout this paper. Finally, we describe the basic mechanisms of several GNN algorithms.

2.1 Empirical Analysis

We conduct an empirical study to show the ratio of non-zero elements of each dataset. Firstly, let us define z as below:

$$z = \frac{\# \text{ of non-zero feature dimension in training nodes}}{\# \text{ of entire feature dimension}} \quad (1)$$

The numerator contains the elements of all training nodes whose values are non-zero. In Figure 2, we describe the z-value of each dataset by varying the range of neighbors from ego to 2-hop adjacent nodes. We can see that the z-value increases in proportion to the range since more features are available during the training phase. We also observe that the z-values of datasets are quite different. As we will explain later, the experimental results show that the lower the z-value of a dataset is, the greater the performance improvement that flipping achieves. We insist that the z-value of ego is dominant for gradient updates (see Section 4.6 for details).

2.2 Notations

Let $\mathcal{G} = (\mathcal{V}, \mathcal{E})$ be an undirected graph that contains $|\mathcal{V}| = n$ nodes and $|\mathcal{E}| = m$ edges. Let $A \in \{0, 1\}^{n \times n}$ be an adjacency matrix determined by the connectivity of a graph. In many cases, it is available to utilize a feature matrix $X \in \mathbb{R}^{n \times F}$ that comprise the properties of the entire nodes, where F is the input dimension of initial features. Each node has its label that is represented as $Y \in \mathbb{R}^{n \times C}$. Here, C is the number of labels (classes). We separate the first layer weight matrix of GNN into two parts W_o and W_f , where the lower script o and f denote an original and flipped space, respectively. A symbol ∇ represents a partial derivative. Our goal is to solve a node classification task under semi-supervised settings, where the labeled nodes $\mathcal{V}_L \subset \mathcal{V}$ are partially available as a training set. GNNs focus on how to better utilize the given information for the prediction of unlabeled nodes $\mathcal{V}_U = \mathcal{V} - \mathcal{V}_L$.

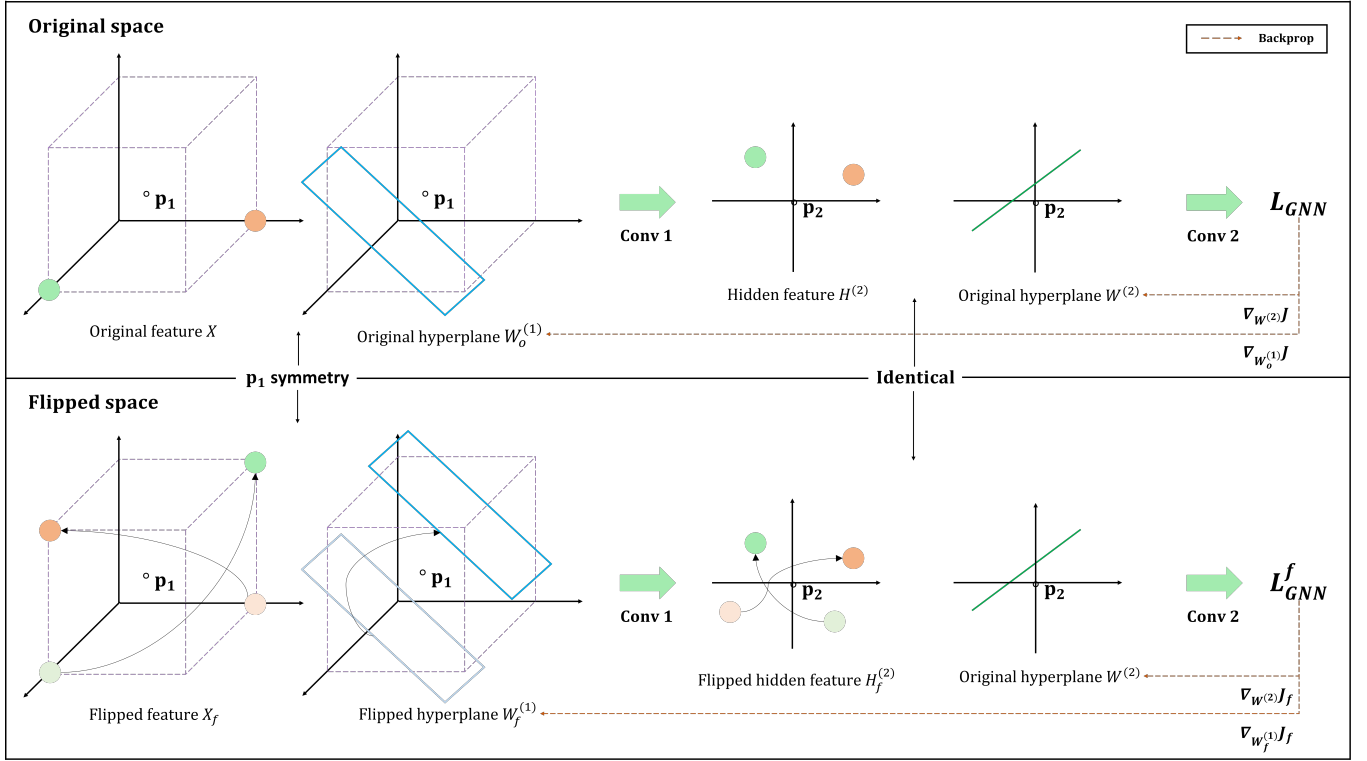


Figure 3: The overall architecture of Flip-GCN. The hyperplanes are updated iteratively using both features

2.3 Basic GNN Mechanism

We focus on spatial GNNs which can reduce the computational cost of Laplacian decomposition. Their basic form is as below:

$$H^{(l+1)} = \sigma(\tilde{H}^{(l+1)}), \quad \tilde{H}^{(l+1)} = \hat{A}H^{(l)}W^{(l)} \quad (l \geq 1) \quad (2)$$

$$\hat{Y} = \text{softmax}(\tilde{H}^{(L)}).$$

\hat{A} stands for a matrix that is used for message passing. $H^{(1)} = X$ is an initial feature of nodes and $H^{(l)}$ is their representations at the l -th hidden layer. $\tilde{H}^{(l)}$ is a vector at the l -th layer before activation σ (e.g., ReLU). Applying softmax on the output $\tilde{H}^{(L)}$, GNNs obtain the final prediction. $W^{(l)}$ is the trainable weight matrices at the l -th layer shared across all nodes. They are updated through negative log-likelihood loss \mathcal{L}_{nll} between the predicted \hat{Y} and true labels Y as below:

$$\mathcal{L}_{GNN} = \mathcal{L}_{nll}(Y, \hat{Y}). \quad (3)$$

GNNs [1, 6, 26, 41] have their unique aggregation schemes (finding appropriate \hat{A}). For example, GCN [25] takes the normalized Laplacian $\hat{A} = \tilde{D}^{-0.5}\tilde{A}\tilde{D}^{-0.5}$ and GAT [41] constructs an aggregation matrix by computing attention score between two nodes i, j as below:

$$\hat{A}_{ij} = \frac{\exp(\sigma(a[h_i||h_j]))}{\sum_{k \in N_i} \exp(\sigma(a[h_i||h_k]))}. \quad (4)$$

Layer-wise attention is used, but we omit it for brevity. Others [21] compute an additional matrix A^s based on the similarities of all node pairs, and integrate them with the original adjacency matrix

A as below:

$$\hat{A} = pA + (1-p)A^s, \quad A_{ij}^s = \frac{x_i^T x_j}{\|x_i\| \|x_j\|} \quad (5)$$

, where p balances weights between A and A^s .

3 METHODOLOGY

We first explain the limitation of the generic GNN mechanism. It is undeniable that appropriate aggregation schemes are essential for securing the proper performance of GNNs. However, as explained below, an aggregation scheme alone cannot avoid the improper learning problem rooted in the sparseness of the initial features. To explain the problem in greater detail, we first scrutinize the backpropagation of GNNs:

$$\nabla_{W^{(l)}} J = (\hat{A}H^{(l)})^T \nabla_{\tilde{H}^{(l+1)}} J, \quad l = 1, \dots, L. \quad (6)$$

Here, $J = \mathcal{L}_{GNN}$ represents a full-batch gradient of Equation 3. As can be seen in the above equation, the sparseness (or low value) of \hat{A} can obstruct the gradient flow between dissimilar nodes. Unfortunately, there arises a problem when updating the parameters of initial layer $W^{(1)}$ as:

$$\begin{aligned} \nabla_{W^{(1)}} J &= (\hat{A}H^{(1)})^T \nabla_{\tilde{H}^{(2)}} J \\ &= (\hat{A}X)^T \nabla_{\tilde{H}^{(2)}} J. \end{aligned} \quad (7)$$

The above equation implies that the gradients become zero for certain dimensions with zero inputs (please refer to Figure 1a). Thus,

aggregation itself cannot handle the precise update of the first hyperplane $W^{(1)}$, necessitating a sparseness removal mechanism for the initial features X . To enable $W^{(1)}$ to learn the precise meaning of each dimension, we suggest flipping which is simple but is effective for semi-supervised learning. In the upcoming subsection, we detail the training mechanism of GCN in the flipped space accompanied by parameter adjustment.

3.1 Flipped Graph Neural Networks

The inadequate gradient update problem described before can be more conspicuous in semi-supervised learning. A simple remedy to the problem is shifting which is popularly used in computer vision. To remove zero signals, shifting adds a vector X_s , which consists of elements of small values, to the input features X as below:

$$X = X + X_s. \quad (8)$$

However, shifting may not be applicable to GNNs because MLP is not shift-invariant and can deteriorate robustness [39]. Further, it changes the magnitude of an input which is critical to the normalization of neural networks. For a more rigorous investigation on shifting, we devise a simple method that combines shifting with GCN and describes their performance in Appendix B.

We develop a scheme that flips both feature vectors and the hyperplane concurrently. If an original feature all of whose elements belong to $[0, 1]$, its symmetric transposition through $p = (0.5, \dots, 0.5)$ also resides in this range. (See the hypercube in the upper, left-most graphs in Figure 3 where a red point $(1,0,0)$ transpositions to $(0,1,1)$) This transposition is also applicable to the hyperplane $W^{(1)}$. In Figure 3, the upper and lower panels describe the original and flipped spaces, respectively. Even though the proposed flipping scheme is orthogonal to GNN techniques, We take GCN as a convolution layer as defined in Eq. 2. We apply flipping to MLP and GAT and obtain Flip-MLP and Flip-GAT as demonstrated in Appendix D.

Original space. Back to Figure 3, the upper panel is the same as plane GCN [25]. The last row and column of X and $W^{(1)}$ are zero-padded as below (this will be explained later):

$$X[F:] = 0, \quad W_o^{(1)} = \begin{pmatrix} W^{(1)} \\ 0 \end{pmatrix}. \quad (9)$$

Then, using Eq. 2 and 3 we can update the model's parameters.

Before introducing the flipped space, we first define some symbols. $p_1 = (0.5, \dots, 0.5, 0) \in \mathcal{R}^{F+1}$ and $p_2 = (0, \dots, 0) \in \mathcal{R}^{F'}$ are two datum points that are used for flipping. The last dimension of p_1 is zero-padded to be in line with $X \in \mathcal{R}^{n \times (F+1)}$ and $W^{(1)} \in \mathcal{R}^{(F+1) \times F'}$ where F and F' are the dimensions of the initial feature and the vector after the first projection, respectively. Reasons for the selection of these points (p) are described in Section 3.3.

Flipped space. The flipped features X_f are obtained by transposing the original features X through p_1 as below:

$$X_f = 2p_1 - X. \quad (10)$$

We should also flip the first hyperplane $W^{(1)}$ as described in Figure 4a. Firstly, we need to calculate a distance vector $d \in \mathcal{R}^{F'}$ between

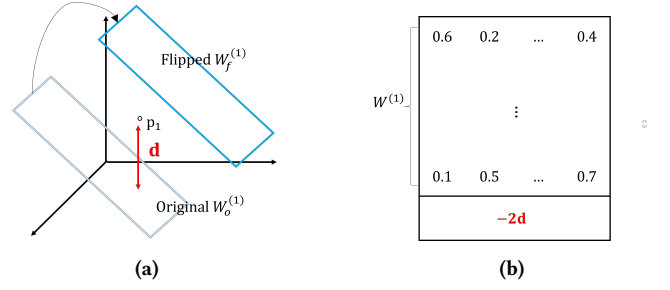


Figure 4: (a) Distance d from $W_o^{(1)}$ to p_1 . (b) $W_f^{(1)}$ is retrieved by padding $-2d$ to the last dimension of $W^{(1)}$

Algorithm 1 The overall mechanism of Flip-GCN

Require: Adjacency matrix A , node features X , parameters θ_G , epoch K , best valid and test acc. $\gamma' = \delta' = 0$, learning rate η

Ensure: Node classification accuracy δ'

- 1: **for** number of training epoch K **do**
 - 2: # GCN in original space
 - 3: **for** training samples **do**
 - 4: Using initial features X , compute the \mathcal{L}_{GNN} (Eq. 3)
 - 5: Update $\theta_G^{k+1} = \theta_G^k - \eta \frac{\partial \mathcal{L}_{GNN}}{\partial \theta_G^k}$
 - 6: **end for**
 - 7: Compute the validation γ and test score δ
 - 8: **if** $\gamma > \gamma'$ **then**
 - 9: $\gamma' = \gamma, \delta' = \delta$
 - 10: # GCN in flipped space
 - 11: **for** training samples **do**
 - 12: Flip initial features using Eq. 10
 - 13: Flip the first hyperplane through Eq. 11
 - 14: Using these parameters, compute \mathcal{L}_{GNN}^f in Eq. 13
 - 15: Update $\theta_G^{k+2} = \theta_G^{k+1} - \eta \frac{\partial \mathcal{L}_{GNN}^f}{\partial \theta_G^{k+1}}$
 - 16: **end for**
 - 17: Compute the validation γ and test score δ
 - 18: **if** $\gamma > \gamma'$ **then**
 - 19: $\gamma' = \gamma, \delta' = \delta$
 - 20: **end for**
-

the original hyperplane $W_o^{(1)}$ and p_1 as follows:

$$d = \sum_{j=0}^F (p_1 \otimes W_o^{(1)})[:, j], \quad (11)$$

$$W_f^{(1)} = \begin{pmatrix} W^{(1)} \\ -2d \end{pmatrix}$$

, where \otimes is an element-wise product. Referring to Figure 4b, $W_f^{(1)}$ is retrieved by padding $-2d$ to the last element. We can assure the p_2 (origin) symmetry after the first convolution as $XW_o^{(1)} = -X_fW_f^{(1)}$. In the flipped space, we should also flip the sign of the output

Table 1: Statistical details of nine benchmark graph datasets

Datasets	Cora	Citeseer	Pubmed	Actor	Chameleon	Squirrel	Cornell	Texas	Wisconsin
# Nodes	2,708	3,327	19,717	7,600	2,277	5,201	183	183	251
# Edges	10,558	9,104	88,648	25,944	33,824	211,872	295	309	499
# Features	1,433	3,703	500	931	2,325	2,089	1,703	1,703	1,703
# Classes	7	6	3	5	5	5	5	5	5
# Training Nodes	140	120	60	100	100	100	25	25	25
# Validation Nodes	1,568	2,207	18,657	3,750	1,088	2,550	79	79	113
# Test Nodes	1,000	1,000	1,000	3,750	1,089	2,551	79	79	113

$\sigma(\widehat{A}X_f W_f^{(1)})$ before the next convolution layer as follows:

$$\begin{aligned} H_f^{(2)} &= -\sigma(\widehat{A}X_f W_f^{(1)}), \quad (l=1) \\ H_f^{(l+1)} &= \sigma(\widehat{H}_f^{(l+1)}), \quad \widehat{H}_f^{(l+1)} = \widehat{A}H_f^{(l)} W_f^{(l)}, \quad (l \geq 2) \end{aligned} \quad (12)$$

The loss \mathcal{L}_{GNN}^f can be computed using the final representation $\widehat{H}_f^{(L)}$ as below:

$$\mathcal{L}_{GNN}^f = \mathcal{L}_{nll}(Y, \widehat{Y}_f), \quad \widehat{Y}_f = \text{softmax}(\widehat{H}_f^{(L)}). \quad (13)$$

Based on Eq. 13, $W^{(1)}$ can be trained in the flipped space. We describe the mechanism of our method in Algorithm 1.

3.2 Optimization Strategy

We define two loss functions in Equation 3 and 13. For gradient analyses, it is worth noting the following equation:

$$H^{(2)} = \sigma(\widehat{A}X W_o^{(1)}) = H_f^{(2)} = -\sigma(\widehat{A}X_f W_f^{(1)}) \quad (14)$$

, which implies that the outputs (or gradients) of two different spaces are equivalent after two layers as below:

$$\nabla_{W_o^{(l)}} J = \nabla_{W_f^{(l)}} J_f, \quad (l \geq 2). \quad (15)$$

Similar to J , $J_f = \mathcal{L}_{GNN}^f$ is a full-batch gradient in the flipped space (Eq. 13). Even though Sigmoid or Tanh guarantees a perfect symmetry $J = J_f$, we employ ReLU for better performance. Now, referring to Eq. 7, we define the gradients of the first hyperplane $W^{(1)}$ on both spaces as below.

In the original space, update $W_o^{(1)}$:

$$\nabla_{W_o^{(1)}} J = (\widehat{A}X)^T \nabla_{\widehat{H}^{(2)}} J, \quad \widehat{H}^{(2)} = \widehat{A}X W_o^{(1)}. \quad (16)$$

In the flipped space, update $W_f^{(1)}$:

$$\nabla_{W_f^{(1)}} J_f = (\widehat{A}X_f)^T \nabla_{\widehat{H}_f^{(2)}} J_f, \quad \widehat{H}_f^{(2)} = \widehat{A}X_f W_f^{(1)}. \quad (17)$$

Through the above equations, we can guide the first hyperplane $W^{(1)}$ concurrently.

Convergence analysis. We show that our optimization guarantees the convergence of $W^{(1)}$. If the activation function is origin symmetric, we can redefine Eq. 16 and 17 as below:

$$\begin{aligned} \nabla_{W^{(1)}} J &= (\widehat{A}X)^T \nabla_{\widehat{H}^{(2)}} J, \\ \nabla_{W^{(1)}} J_f &= -(\widehat{A}(2p_1 - X))^T \nabla_{\widehat{H}^{(2)}} J. \end{aligned} \quad (18)$$

Here, the gradient of each dimension in $W^{(1)}$ is proportional to X and $X - 2p_1$ in the original and the flipped spaces. Also, it gets closer to a local optimum $W_*^{(1)}$ as the iteration T increases $\mathbb{E}[W_T^{(1)} - W_*^{(1)}]^2 \propto \frac{\log T}{T}$ [27], and this theorem shows that two-layer neural networks with a ReLU activation converge to a local minimum. Note that gradient ∇J and parameters $|W^{(l)}|, |W_f^{(l)}|$ are all bounded. These properties guarantee the convergence of Flip-GCN [5]. Further, we find that restricting the scale of gradients (α, β) in two spaces can generalize our model as below:

$$W_o^{(1)} = W_o^{(1)} - \alpha \nabla_{W_o^{(1)}} J, \quad W_f^{(1)} = W_f^{(1)} - \beta \nabla_{W_f^{(1)}} J_f \quad (19)$$

3.3 Design Choice

Though plane GNN guarantees the convergence to a local optimum, the initial features might incur overfitting in the first hyperplane. Consequently, GNNs may fail to learn the meaning of entire dimensions when bag-of-words are adopted as features. As described in Eq. 8, shifting might be one solution but it raises a difficult regularization issue. Therefore, we devise flipping which preserves the scale of initial features before and after transposition. We further pick p_1 as an anchor point such that the first hyperplane can be trained concurrently from both spaces.

3.4 Time Complexity

To analyze the computational complexity, we divide our model into two parts. As demonstrated in Figure 3, the proposed scheme consists of a vanilla GCN [25] and a flipped GCN. The computational cost of vanilla GCN is known to be $\mathcal{O}(|\mathcal{E}|P_{GCN})$, where P_{GCN} and is the number of learnable weights. More specifically, P_{GCN} can be decomposed [51] into $\mathcal{O}(nz(X)F' + F'C)$, where $nz(X)$ is the number of non-zero elements in input X and F' is the dimension after projection. $F'C$ is the parameter of the second convolution layer. Also, $\mathcal{O}|\mathcal{E}| \approx \mathcal{O}|\mathcal{E}|d_{max}$ and d_{max} is the maximum degree. Similar to the vanilla GCN, the complexity of the flipped GCN can be defined as $\mathcal{O}(|\mathcal{E}|P'_{GCN})$. In detail, $P'_{GCN} = \mathcal{O}(nz(X_f)F' + F'C)$ where $nz(X_f)$ is the number of non-zero elements in flipped features. Summarizing the above two equations, the complexity of our model is $\mathcal{O}(|\mathcal{E}|(P_{GCN} + P'_{GCN}))$, which is proportional to the number of edges $(|\mathcal{E}|)$ and the size of learnable matrices $(P_{GCN} + P'_{GCN})$.

Table 2: Node classification accuracy (%) on benchmark datasets. Bold with an asterisk (*) symbol indicates the best performance, and methods with † are built upon GCN. We show α, β that achieves the best accuracy which is defined in Eq. 19

Datasets	Cora	Citeseer	Pubmed	Actor	Chameleon	Squirrel	Cornell	Texas	Wisconsin
z-value (Eq. 1)	0.59	0.41	0.96	0.21	1.0	1.0	0.62	0.41	0.53
Homophily (Eq. 20)	0.81	0.74	0.8	0.22	0.23	0.22	0.11	0.06	0.16
MLP	53.2 ± 0.5 %	53.7 ± 1.7 %	69.7 ± 0.4 %	27.9 ± 1.1 %	41.2 ± 1.8 %	26.5 ± 0.6 %	60.1 ± 1.2 %	65.8 ± 5.0 %	73.5 ± 5.4 %
GCN [†]	79.1 ± 0.7 %	67.5 ± 0.3 %	77.8 ± 0.2 %	20.4 ± 0.6 %	49.4 ± 0.7 %	31.8 ± 0.9 %	39.4 ± 4.3 %	47.6 ± 0.7 %	40.5 ± 1.9 %
DropEdge [†]	79.0 ± 0.5 %	67.4 ± 0.2 %	77.0 ± 0.3 %	20.2 ± 0.4 %	48.9 ± 1.1 %	30.9 ± 0.8 %	46.7 ± 3.5 %	47.5 ± 2.6 %	43.3 ± 4.6 %
Ortho-GCN [†]	80.6 ± 0.4 %	69.5 ± 0.3 %	76.9 ± 0.3 %	21.4 ± 1.6 %	46.7 ± 0.5 %	31.3 ± 0.6 %	45.4 ± 4.7 %	53.1 ± 3.9 %	46.6 ± 5.8 %
GIN	77.3 ± 0.8 %	66.1 ± 0.6 %	77.1 ± 0.7 %	24.6 ± 0.8 %	49.1 ± 0.7 %	28.4 ± 2.2 %	42.9 ± 4.6 %	53.5 ± 3.0 %	38.7 ± 0.5 %
GAT	80.1 ± 0.6 %	68.0 ± 0.7 %	78.0 ± 0.4 %	22.5 ± 0.3 %	46.9 ± 0.8 %	30.8 ± 0.9 %	42.1 ± 3.1 %	49.2 ± 4.4 %	45.8 ± 5.3 %
GATv2	79.5 ± 0.5 %	67.4 ± 0.6 %	76.2 ± 0.5 %	22.1 ± 2.0 %	48.3 ± 0.4 %	28.9 ± 1.2 %	38.0 ± 3.8 %	52.5 ± 1.7 %	41.7 ± 5.1 %
APPNP	81.9 ± 0.4 %	68.9 ± 0.3 %	79.0 ± 0.4 %	21.5 ± 0.2 %	45.0 ± 0.5 %	30.3 ± 0.6 %	49.8 ± 3.6 %	56.1 ± 0.2 %	45.7 ± 1.7 %
GCNII	79.6 ± 0.7 %	67.0 ± 1.4 %	77.8 ± 0.4 %	26.1 ± 1.2 %	45.1 ± 0.5 %	28.1 ± 0.7 %	62.5 ± 0.5 %	69.3 ± 2.1 %	63.2 ± 3.0 %
H2GCN	79.5 ± 0.6 %	67.4 ± 0.5 %	78.7 ± 0.3 %	25.8 ± 1.2 %	47.3 ± 0.9 %	31.1 ± 0.5 %	59.8 ± 3.7 %	66.3 ± 4.6 %	61.5 ± 4.4 %
P-reg [†]	80.0 ± 0.8 %	69.2 ± 0.7 %	77.4 ± 0.4 %	20.9 ± 0.5 %	49.1 ± 0.1 %	33.6* ± 0.4 %	44.9 ± 3.1 %	58.5 ± 4.2 %	53.7 ± 2.6 %
FAGCN	81.0 ± 0.3 %	68.3 ± 0.6 %	78.9 ± 0.4 %	26.7 ± 0.8 %	46.8 ± 0.6 %	29.9 ± 0.5 %	46.5 ± 1.7 %	53.8 ± 1.2 %	51.0 ± 4.1 %
Flip-MLP	61.4 ± 0.7 %	60.3 ± 0.5 %	74.1 ± 0.5 %	35.9* ± 0.5 %	43.5 ± 1.2 %	28.5 ± 0.8 %	70.5* ± 4.1 %	79.2* ± 3.6 %	80.5* ± 5.1 %
vs MLP (+ %)	+ 15.4 %	+ 12.1 %	+ 6.3 %	+ 28.7 %	+ 2.3 %	+ 2.1 %	+ 17.3 %	+ 20.4 %	+ 9.5 %
α, β	1, 0.1	1, 1	1, 0.01	0.1, 0.1	1, 1	1, 1	0.1, 0.1	0.1, 0.01	1, 1
Flip-GCN [†]	82.7 ± 0.5 %	72.4 ± 0.4 %	79.2* ± 0.2 %	28.6 ± 0.3 %	50.4* ± 0.5 %	32.4 ± 0.3 %	52.4 ± 0.6 %	62.2 ± 1.8 %	52.3 ± 2.4 %
vs GCN (+ %)	+ 4.6 %	+ 7.3 %	+ 1.8 %	+ 40.2 %	+ 2.0 %	+ 1.9 %	+ 33.0 %	+ 30.7 %	+ 29.1 %
α, β	0.1, 0.01	0.001, 0.001	1, 0.01	0.1, 0.1	1, 0.0001	1, 1	0.01, 0.1	0.1, 0.01	0.1, 1
Flip-GAT	83.1* ± 0.6 %	72.8* ± 0.4 %	78.5 ± 0.2 %	30.3 ± 0.8 %	48.3 ± 0.3 %	31.9 ± 0.5 %	50.6 ± 1.4 %	61.0 ± 1.1 %	54.5 ± 2.1 %
vs GAT (+ %)	+ 3.7 %	+ 7.1 %	+ 0.6 %	+ 34.7 %	+ 3.0 %	+ 3.6 %	+ 20.2 %	+ 22.0 %	+ 19.0 %
α, β	0.1, 0.01	0.01, 0.001	1, 0.001	0.1, 0.1	1, 0.01	1, 1	0.1, 0.01	0.1, 0.01	0.1, 0.01

4 EXPERIMENTS

This section describes the experiments for the performance analysis. We focused our efforts to find answers to the following research questions:

- **RQ1:** Does flipping efficiently solve the problem occurred by multiple zero values in initial features?
- **RQ2:** Does flipping preserve the convergence?
- **RQ3:** How does the performance of the flipping method change as the number of training samples vary?
- **RQ4:** How much do the gradients from the original and flipped spaces differ?

4.1 Datasets and Baselines

Details of datasets. Our experiments are conducted on nine datasets whose statistical details are described in Table 1. We also measure the assortativity of each dataset as below:

$$h = \frac{\# \text{ of edges that connect nodes with the same label}}{\# \text{ of entire edges}} \quad (20)$$

- **Cora, Citeseer, Pubmed** [25] These datasets are citation networks. Here, a node is a single paper and an edge from one paper to another represents a citation. The original graph is directed, but here, we ignore directions. The node features of Cora and Citeseer are the bag-of-words (binary) while Pubmed consists of zero and TF-IDF values. The labels are the topic of the papers.
- **Actor** [40] This dataset is an actor co-occurrence graph, where a node represents an actor and edges are the co-occurrence of two actors in the same movie. The node feature

encodes the keywords in the actor’s Wikipedia web pages, and thus, it only comprises binary values. Labels are five types of actors determined from keywords.

- **Chameleon, Squirrel** [37] These graphs are from Wikipedia web pages. The node features are the vector of several informative nouns, where all elements have non-zero positive or negative values. The maximal element of each dataset is 46.4 and 70.4, while the minimum values are -0.57 and -0.99 which can be inappropriate for our method. The edges are hyperlinks between web pages. Web pages are classified into five types (labels) based on the monthly traffic.
- **Cornell, Texas, Wisconsin**¹ The WebKB datasets include web pages that are collected from computer science departments of multiple universities. Here, the nodes are web pages and the edges are hyperlinks between them. Similar to citation networks and actor graphs, the node features are binary values (bag-of-words) and their labels are manually classified as the student, faculty, staff, course, and project.

Baselines We compare our proposed method with several state-of-the-art baselines below.

- **MLP** [35] adopts a feed-forward neural network without using neighboring nodes.
- **GCN** [25] is a first-order approximation of Chebyshev polynomials [9] that utilizes localized filters.
- **DropEdge** [36] randomly deletes edges based with a given probability in order to alleviate over-fitting.

¹<http://www.cs.cmu.edu/afs/cs/project/theo-20/www/data/>

- **Ortho-GCN** [17] maintains the orthogonality of feature transformation matrices through three constraints.
- **GIN** [45] adopts an injective mapping function to enhance the discriminative power of GCN and ensures isomorphism.
- **GAT** [41] employs node features to assign different weights for each edge without graph structural property.
- **GATv2** [2] improves GAT to generate a more dynamic graph attention that is more expressive.
- **APPNP** [26] combines personalized PageRank with GCN to improve accuracy while reducing a computational cost.
- **GCNII** [6] further utilizes weighted identity mapping function to redeem the deficiency of APPNP.
- **H₂GCN** [51] separates ego from neighbors and apply hop-based aggregation for heterophilic networks.
- **P-reg** [47] improves the traditional graph Laplacian to provide extra information that GNNs might not capture.
- **FAGCN** [1] adaptively controls the propagation of low and high frequency signals during message passing.

4.2 Experiment Details

We implemented the baselines and our method using *PyTorch Geometric*² [13]. In detail, two layers of GNNs are used for all baselines except for APPNP and GCNII. The hidden dimension is set to 64 and we adopted ReLU as an activation function with dropout. The log Softmax is applied for classification. A learning ratio of ($1e^{-3}$) and Adam optimizer with weight decay ($5e^{-4}$) are used for training. As illustrated in Table 1, we randomly chose 20 nodes per class as training samples except for the WebKB datasets whose size is smaller than the others. The remaining nodes are randomly and equally divided into validation and testing nodes. The test accuracy is measured at each iteration, and we selected one that achieves the best validation score. Our source code is available *here*³. In addition to flip-GCN, we describe the details of Flip-MLP and Flip-GAT in Appendix D.

4.3 Results and Discussion (RQ1)

Most importantly, in Table 2, we notice that the three flipping variants (Flip-MLP, Flip-GCN, and Flip-GAT) perform significantly better than their bases (MLP, GCN, and GAT). Now, we analyze these results from two perspectives.

Performance of flipping is sensitive to the z-value. Because flipping is designed to reduce overfitting caused by the sparsity in initial features, we can easily presume that z-value, the non-zero element ratio, is the key factor that determines the performance gains of flipping. Indeed, flipping attains larger performance gains on low z-value datasets than on high z-value datasets. For three datasets with high z-values (Pubmed, Chameleon, and Squirrel), the advancement of flipping over their vanilla models (e.g., Flip-MLP vs MLP) is relatively small. However, all three flipping methods perform better than the original methods achieving average gains of 3 %, 1.9 %, and 2.4 %, respectively, indicating the effectiveness of flipping even for non-zero initials. On another dataset with low z-values, the three flipping variants obtain remarkable advancements

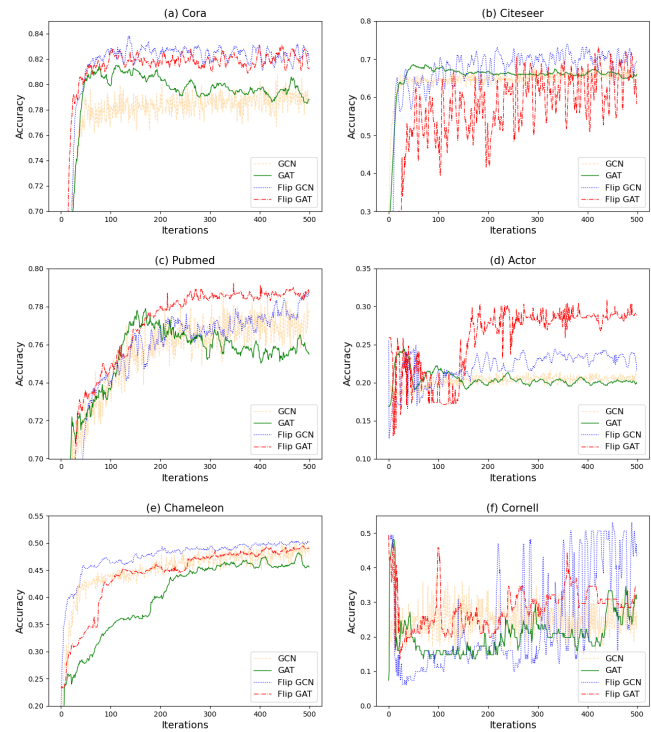


Figure 5: Performance of four methods as a function of the number of iterations

over their bases achieving 17.2 %, 24.2 %, and 17.8 % on average. Notably, flipping methods perform best except for Squirrel (with high z and low homophily). This may imply that a slight perturbation to the input features can have a greater impact than aggregation scheme modifications under semi-supervised settings.

The accuracy of GNNs are highly related to the homophily ratio. Message passing based GNNs exploit the homophily (Eq. 20) property commonly observed in graphs [28, 46]. Three citation graphs have higher homophily ratios (≥ 0.7) than others. Here, GNNs overwhelm MLP on these homophilic graphs. However, in other datasets like Actor and three WebKB networks, Flip-MLP achieves the best accuracy among the baselines. This implies that message passing fails to generalize well under the high heterophily. Further, the performance gain of Flip-MLP is higher than Flip-GNNs on homophilic graphs, but on heterophilic graphs, GNNs better benefit from the advantages of flipping. Among baselines, APPNP performs best on homophilic graphs and some methods (H₂GCN, FAGCN) outperform GCN on heterophilic networks. However, our flipping methods surpass these algorithms regardless of homophilic ratios.

4.4 Convergence Analysis (RQ2)

One may argue that flipping may hurt the stability of flipping because it operates on two spaces. Figure 5 plots the performance of two baselines (GCN and GAT) and two flipping methods (Flip-GCN and Flip-GAT) as a function of the number of iterations (only

²<https://pytorch-geometric.readthedocs.io/en/latest/modules/nn.html>

³<https://anonymous.4open.science/r/Flip-GCN-9870>

Table 3: Node classification accuracy (%) w.r.t. the different number of training samples

Dataset	Cora			Citeseer		
	L/C	20	40	80	20	40
z-value	0.59	0.91	0.9	0.41	0.59	0.78
MLP	53.2	56.9	62.1	53.7	57.3	63.8
Flip-MLP	61.4	65.5	70.4	60.3	63.1	67.7
GCN	79.1	82.8	83.4	67.5	69.3	71.5
Flip-GCN	82.7	84.5	85.5	72.4	73.3	75.6
GAT	80.1	82.4	83.0	68.0	68.9	71.5
Flip-GAT	83.1	84.0	84.6	72.8	73.4	74.3

six datasets are illustrated due to the space limit). The performance of plain GCN (orange), plain GAT (green), flip-GCN (blue), and flip-GAT (red) are plotted with different colors. Here, the x-axis is the training epoch and the y-axis is node classification accuracy.

Back into Figure 5, we can see that the flipped methods generally outperform the plain algorithms. Also, compared to the plane GCN and GAT, we notice that flip-based methods experience higher oscillations. We contemplate that this is caused by the gradient updates in the flipped space, where most dimensions are updated at each iteration. Even though flipping methods achieve better performance than the plain models after 100 to 200 epochs, they suffer from larger instability leaving further investigation on this issue.

4.5 Varying the Size of Training Samples (RQ3)

As we pointed out before, the root cause that deteriorates the performance of semi-supervised learning is the lack of labeled samples. Thus, we scrutinize the effect of labeled sample size on performance by adjusting the scale of training samples. In Table 3, we show the z-value of central nodes based on the number of labeled nodes per class (L/C). Due to the space limitation, we only describe Cora and Citeseer cases here. More experimental results can be found in Appendix C.

From the above result, GCN and GAT outperform MLP since the above two datasets are quite assortative (please see Homophily in Table 2). At the same time, we can observe that the performance gain of flipping decreases as the L/C increases. The reason is that as more training nodes are available, the initial features start to cover most dimensions (large z-value) such that plain models can update the first weight matrix. As described in Table 5 (Appendix C), for some datasets (Chameleon, Squirrel) whose entire features are non-zero, we notice that flip merely affect the overall quality as the number of samples increase.

4.6 Analysis of Gradients on Two Spaces (RQ4)

Figure 6 analyzes the gradient of the first projection matrix during the training phase with the Cora dataset. We apply different ranges of neighboring nodes and define four types. The first one (T1) only comprises features of central nodes (Ego). T2 and T3 include features of 1-hop and 2-hop neighbors, respectively. The final (T4) consists of leftover features. We prioritize the types from T1 to T4 to avoid overlapped features being double-counted. Note that all $T \in \mathcal{R}^F$ are binarized.

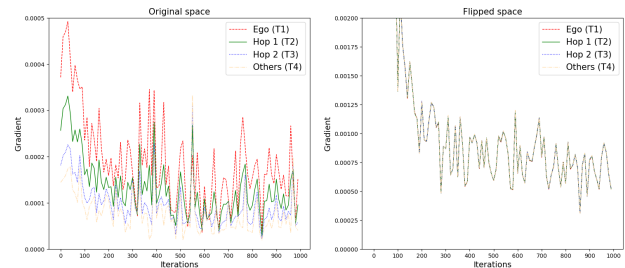


Figure 6: Using the Cora dataset, we plot the magnitude of the first projection matrix gradients during the training phase as a function of the number of iterations

In Figure 6, we averaged the magnitude of gradients in two spaces and plot them with different colors. In the original space (left), the features from T1 (red) receive the largest gradient. As described in Eq. 6, the gradients of a neighbor are inversely proportional to its degree. T4 (orange) shows the smallest values suggesting that features are mostly excluded during training (the weight regularization slightly updates the parameters). On the other hand, in flipped space (right), all types tend to have a similar magnitude that conforms to our suggestions; large losses in the flipped space bring large gradients. Thus, we need to adjust them through Eq. 19 during backward propagation.

5 RELATED WORK

Graph Neural Networks. Under semi-supervised settings, GNNs have achieved substantial improvement for many tasks including node and graph classifications. Generally, most of them can be classified into two types; spectral-based and spatial-based algorithms. The first one established a mathematical foundation of conducting graph convolution operation in a spectral domain using the Laplacian matrix [3, 9, 10]. Spatial-based GNNs aggregate the information of local neighborhoods from spatial perspectives, and ignited many aggregation scheme developments for the handling of noisy connections [1, 8, 34, 41, 51]. Compared to the noisy neighbor problem, the problem incurred by the sparse initial features has not received much research attention.

Generalization of neural networks. Many approaches have been proposed for the generalization of parameters in neural networks [5, 12, 43]. Several suggested the normalization of deep neural networks [19] while others applied regularization to all adjacent nodes [47] or integrated label propagation to give further information [42]. More recently, the orthogonal GCN [17] attacks the gradient vanishing problem at the initial few layers of GNNs. Rawls-GCN [22] claims the unfairness of gradient update which is biased to nodes with a large degree. Though these methods show notable improvements under the semi-supervised scenario, they fail to solve the problem that is inherently occurred by a characteristic of initial features. In this paper, we aim to solve this limitation through the generalization of the first hyperplane.

6 CONCLUSION

Existing GNNs mainly focus on the tuning of aggregation strategy, while the type of initial features is unconsidered. In this work, we investigate the theoretical relationship between the zero elements of input vectors and their impact on the first layer of neural networks. We then propose a co-training in both the original and flipped spaces, which learns the gradient flows from both channels and adaptively adjusts the parameters. We provide an analysis of the backpropagation and empirical studies on nine real-world benchmark datasets. Equipping three base methods with flipping improves the node classification accuracy, which indicates that our suggestion is highly scalable and competitive. In future work, we expect the application of flipping with many other variations of GNNs to enhance their quality.

REFERENCES

- [1] Deyu Bo, Xiao Wang, Chuan Shi, and Huawei Shen. 2021. Beyond low-frequency information in graph convolutional networks. *arXiv preprint arXiv:2101.00797* (2021).
- [2] Shaked Brody, Uri Alon, and Eran Yahav. 2021. How attentive are graph attention networks? *arXiv preprint arXiv:2105.14491* (2021).
- [3] Joan Bruna, Wojciech Zaremba, Arthur Szlam, and Yann LeCun. 2013. Spectral networks and locally connected networks on graphs. *arXiv preprint arXiv:1312.6203* (2013).
- [4] Tianle Cai, Shengjie Luo, Keyulu Xu, Di He, Tie-yan Liu, and Liwei Wang. 2021. Graphnorm: A principled approach to accelerating graph neural network training. In *International Conference on Machine Learning*. PMLR, 1204–1215.
- [5] Jianfei Chen, Jun Zhu, and Le Song. 2017. Stochastic training of graph convolutional networks with variance reduction. *arXiv preprint arXiv:1710.10568* (2017).
- [6] Ming Chen, Zhewei Wei, Zengfeng Huang, Bolin Ding, and Yaliang Li. 2020. Simple and deep graph convolutional networks. In *International Conference on Machine Learning*. PMLR, 1725–1735.
- [7] Yunpeng Chen, Jianan Li, Huaxin Xiao, Xiaojie Jin, Shuicheng Yan, and Jiashi Feng. 2017. Dual path networks. *Advances in neural information processing systems* 30 (2017).
- [8] Eli Chien, Jianhao Peng, Pan Li, and Olgica Milenkovic. 2020. Adaptive universal generalized pagerank graph neural network. *arXiv preprint arXiv:2006.07988* (2020).
- [9] Michaël Defferrard, Xavier Bresson, and Pierre Vandergheynst. 2016. Convolutional neural networks on graphs with fast localized spectral filtering. *Advances in neural information processing systems* 29 (2016).
- [10] Yushun Dong, Kaize Ding, Brian Jalaian, Shuiwang Ji, and Jundong Li. 2021. Graph neural networks with adaptive frequency response filter. *arXiv preprint arXiv:2104.12840* (2021).
- [11] Wenqi Fan, Yao Ma, Qing Li, Yuan He, Eric Zhao, Jiliang Tang, and Dawei Yin. 2019. Graph neural networks for social recommendation. In *The world wide web conference*. 417–426.
- [12] Jean Feng and Noah Simon. 2017. Sparse-input neural networks for high-dimensional nonparametric regression and classification. *arXiv preprint arXiv:1711.07592* (2017).
- [13] Matthias Fey and Jan Eric Lenssen. 2019. Fast graph representation learning with PyTorch Geometric. *arXiv preprint arXiv:1903.02428* (2019).
- [14] Alex Fout, Jonathon Byrd, Basir Shariat, and Asa Ben-Hur. 2017. Protein interface prediction using graph convolutional networks. *Advances in neural information processing systems* 30 (2017).
- [15] Justin Gilmer, Samuel S Schoenholz, Patrick F Riley, Oriol Vinyals, and George E Dahl. 2017. Neural message passing for quantum chemistry. In *International conference on machine learning*. PMLR, 1263–1272.
- [16] Jonathan Godwin, Michael Schaarschmidt, Alexander Gaunt, Alvaro Sanchez-Gonzalez, Yulia Rubanova, Petar Veličković, James Kirkpatrick, and Peter Battaglia. 2021. Very deep graph neural networks via noise regularisation. *arXiv preprint arXiv:2106.07971* (2021).
- [17] Kai Guo, Kaixiong Zhou, Xia Hu, Yu Li, Yi Chang, and Xin Wang. 2022. Orthogonal graph neural networks. In *Proceedings of the AAAI Conference on Artificial Intelligence*, Vol. 36. 3996–4004.
- [18] Will Hamilton, Zitao Ying, and Jure Leskovec. 2017. Inductive representation learning on large graphs. *Advances in neural information processing systems* 30 (2017).
- [19] Lei Huang, Jie Qin, Yi Zhou, Fan Zhu, Li Liu, and Ling Shao. 2020. Normalization techniques in training dnns: Methodology, analysis and application. *arXiv preprint arXiv:2009.12836* (2020).
- [20] Sergey Ioffe and Christian Szegedy. 2015. Batch normalization: Accelerating deep network training by reducing internal covariate shift. In *International conference on machine learning*. PMLR, 448–456.
- [21] Wei Jin, Tyler Derr, Yiqi Wang, Yao Ma, Zitao Liu, and Jiliang Tang. 2021. Node similarity preserving graph convolutional networks. In *Proceedings of the 14th ACM international conference on web search and data mining*. 148–156.
- [22] Jian Kang, Yan Zhu, Yinglong Xia, Jiebo Luo, and Hanghang Tong. 2022. Rawlsgcn: Towards rawlsian difference principle on graph convolutional network. In *Proceedings of the ACM Web Conference 2022*. 1214–1225.
- [23] Dongkwan Kim and Alice Oh. 2022. How to find your friendly neighborhood: Graph attention design with self-supervision. *arXiv preprint arXiv:2204.04879* (2022).
- [24] Hyungjun Kim, Malte Rasch, Tayfun Gokmen, Takashi Ando, Hiroyuki Miyazoe, Jae-Joon Kim, John Rozen, and Seyoung Kim. 2019. Zero-shifting technique for deep neural network training on resistive cross-point arrays. *arXiv preprint arXiv:1907.10228* (2019).
- [25] Thomas N Kipf and Max Welling. 2016. Semi-supervised classification with graph convolutional networks. *arXiv preprint arXiv:1609.02907* (2016).
- [26] Johannes Klicpera, Aleksandar Bojchevski, and Stephan Günnemann. 2018. Predict then propagate: Graph neural networks meet personalized pagerank. *arXiv preprint arXiv:1810.05997* (2018).
- [27] Yuanzhi Li and Yang Yuan. 2017. Convergence analysis of two-layer neural networks with relu activation. *Advances in neural information processing systems* 30 (2017).
- [28] Derek Lim, Felix Hohne, Xiuyu Li, Sijia Linda Huang, Vaishnavi Gupta, Omkar Bhalerao, and Ser Nam Lim. 2021. Large scale learning on non-homophilous graphs: New benchmarks and strong simple methods. *Advances in Neural Information Processing Systems* 34 (2021), 20887–20902.
- [29] Mingbao Lin, Rongrong Ji, Zihan Xu, Baochang Zhang, Yan Wang, Yongjian Wu, Feiyue Huang, and Chia-Wen Lin. 2020. Rotated binary neural network. *Advances in neural information processing systems* 33 (2020), 7474–7485.
- [30] Hongrui Liu, Binbin Hu, Xiao Wang, Chuan Shi, Zhiqiang Zhang, and Jun Zhou. 2022. Confidence May Cheat: Self-Training on Graph Neural Networks under Distribution Shift. In *Proceedings of the ACM Web Conference 2022*. 1248–1258.
- [31] Dongsheng Luo, Wei Cheng, Wenchao Yu, Bo Zong, Jingchao Ni, Haifeng Chen, and Xiang Zhang. 2021. Learning to drop: Robust graph neural network via topological denoising. In *Proceedings of the 14th ACM International Conference on Web Search and Data Mining*. 779–787.
- [32] Miller McPherson, Lynn Smith-Lovin, and James M Cook. 2001. Birds of a feather: Homophily in social networks. *Annual review of sociology* 27, 1 (2001), 415–444.
- [33] Shashank Pandit, Duen Horng Chau, Samuel Wang, and Christos Faloutsos. 2007. Netprobe: a fast and scalable system for fraud detection in online auction networks. In *Proceedings of the 16th international conference on World Wide Web*. 201–210.
- [34] Hongbin Pei, Bingzhe Wei, Kevin Chen-Chuan Chang, Yu Lei, and Bo Yang. 2020. Geom-gcn: Geometric graph convolutional networks. *arXiv preprint arXiv:2002.05287* (2020).
- [35] Marius-Constantin Popescu, Valentina E Balas, Liliana Perescu-Popescu, and Nikos Mastrokakis. 2009. Multilayer perceptron and neural networks. *WSEAS Transactions on Circuits and Systems* 8, 7 (2009), 579–588.
- [36] Yu Rong, Wenbing Huang, Tingyang Xu, and Junzhou Huang. 2019. Dropedge: Towards deep graph convolutional networks on node classification. *arXiv preprint arXiv:1907.10903* (2019).
- [37] Benedek Rozemberczki, Ryan Davies, Rik Sarkar, and Charles Sutton. 2019. Gemsec: Graph embedding with self clustering. In *Proceedings of the 2019 IEEE/ACM international conference on advances in social networks analysis and mining*. 65–72.
- [38] Jia Shijie, Wang Ping, Jia Peiyi, and Hu Siping. 2017. Research on data augmentation for image classification based on convolution neural networks. In *2017 Chinese automation congress (CAC)*. IEEE, 4165–4170.
- [39] Vasu Singla, Songwei Ge, Basri Ronen, and David Jacobs. 2021. Shift Invariance Can Reduce Adversarial Robustness. *Advances in Neural Information Processing Systems* 34 (2021), 1858–1871.
- [40] Jie Tang, Jimeng Sun, Chi Wang, and Zi Yang. 2009. Social influence analysis in large-scale networks. In *Proceedings of the 15th ACM SIGKDD international conference on Knowledge discovery and data mining*. 807–816.
- [41] Petar Veličković, Guillem Cucurull, Arantxa Casanova, Adriana Romero, Pietro Lio, and Yoshua Bengio. 2017. Graph attention networks. *stat* 1050 (2017), 20.
- [42] Hongwei Wang and Jure Leskovec. 2020. Unifying graph convolutional neural networks and label propagation. *arXiv preprint arXiv:2002.06755* (2020).
- [43] Xiao Wang, Hongrui Liu, Chuan Shi, and Cheng Yang. 2021. Be confident! towards trustworthy graph neural networks via confidence calibration. *Advances in Neural Information Processing Systems* 34 (2021), 23768–23779.
- [44] Teng Xiao, Zhengyu Chen, Donglin Wang, and Suhang Wang. 2021. Learning how to propagate messages in graph neural networks. In *Proceedings of the 27th ACM SIGKDD Conference on Knowledge Discovery & Data Mining*. 1894–1903.
- [45] Keyulu Xu, Weihua Hu, Jure Leskovec, and Stefanie Jegelka. 2018. How powerful are graph neural networks? *arXiv preprint arXiv:1810.00826* (2018).

- [46] Yujun Yan, Milad Hashemi, Kevin Swersky, Yaoqing Yang, and Danai Koutra. 2021. Two sides of the same coin: Heterophily and oversmoothing in graph convolutional neural networks. *arXiv preprint arXiv:2102.06462* (2021).
- [47] Han Yang, Kaili Ma, and James Cheng. 2021. Rethinking graph regularization for graph neural networks. In *Proceedings of the AAAI Conference on Artificial Intelligence*, Vol. 35. 4573–4581.
- [48] Liang Yang, Fan Wu, Yingkui Wang, Junhua Gu, and Yuanfang Guo. 2019. Masked Graph Convolutional Network. In *IJCAI*. 4070–4077.
- [49] Zhitao Ying, Dylan Bourgeois, Jiaxuan You, Marinka Zitnik, and Jure Leskovec. 2019. Gnnexplainer: Generating explanations for graph neural networks. *Advances in neural information processing systems* 32 (2019).
- [50] Xin Zhang, Li Liu, Yuxiang Xie, Jie Chen, Lingda Wu, and Matti Pietikainen. 2017. Rotation invariant local binary convolution neural networks. In *Proceedings of the IEEE International Conference on Computer Vision Workshops*. 1210–1219.
- [51] Jiong Zhu, Yujun Yan, Lingxiao Zhao, Mark Heimann, Leman Akoglu, and Danai Koutra. 2020. Beyond homophily in graph neural networks: Current limitations and effective designs. *Advances in Neural Information Processing Systems* 33 (2020), 7793–7804.
- [52] Yanqiao Zhu, Yichen Xu, Feng Yu, Qiang Liu, Shu Wu, and Liang Wang. 2021. Graph contrastive learning with adaptive augmentation. In *Proceedings of the Web Conference 2021*. 2069–2080.

SUPPLEMENTARY MATERIAL

A FEATURES AND PARAMETER UPDATE

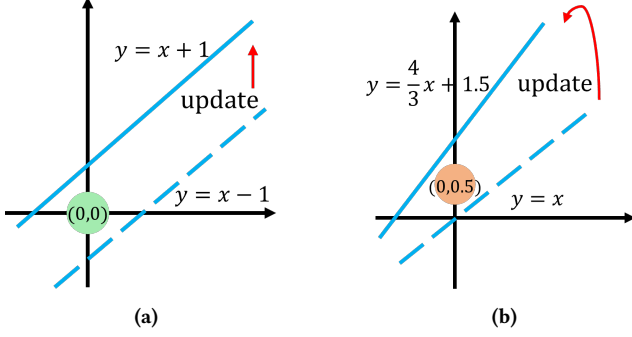


Figure 7: Analysis on gradient update. The dotted line is the line before the update, and the solid one can be derived after backpropagation

In Figure 1, we take two examples using 2-dimensional input data X and a single hyperplane (line) W , respectively. Here, we exclude the activation layer since it is a single layer. Let us assume the true label y of this node is -1. Firstly, we should define the objective function that measures the difference between predicted and true labels. Thus, the prediction and loss calculation in this example can be defined as below:

$$\hat{y} = W^T X = \sum_{i=1}^2 W_i X_i + b,$$

$$\nabla_{W_j} \mathcal{L} = \eta(y - \hat{y}) X_j.$$

Simply, we assume the learning ratio η as 1. Thus, W can be updated as below:

$$\begin{pmatrix} W'_1 \\ W'_2 \end{pmatrix} = \begin{pmatrix} W_1 - X_1(1 - \hat{y}) \\ W_2 - X_2(1 - \hat{y}) \end{pmatrix}$$

, and also bias term as $b' = b - (-1 - \hat{y})$.

Back into Figure 7a, let us assume the initial line is $y = x - 1$. Since the value of input features $X = (0, 0)$, the weights W are not updated. Instead, the bias becomes 1 $b' = -1 - (-1 - 1) = 1$ and successfully predict its label as -1.

Likewise, in Figure 7b, let us consider a line and initial features as $y = x$ and $(0, 0.5)$, respectively. Then, the weights are updated as below:

$$\begin{pmatrix} W'_1 \\ W'_2 \end{pmatrix} = \begin{pmatrix} -1 - 0 * (1 - (0.5)) \\ 1 - 0.5 * (1 - (0.5)) \end{pmatrix} = \begin{pmatrix} -1 \\ 0.75 \end{pmatrix}$$

, and the bias as $0.5 b' = 0 - (-1 - (0.5)) = 1.5$. Consequently, W becomes $y = \frac{4}{3}x + 1.5$ which also classifies this node $(0, 0.5)$ as -1. The main observation is that the update of a hyperplane is quite sensitive to the element of input vectors, even though both of them are well-optimized in the two examples.

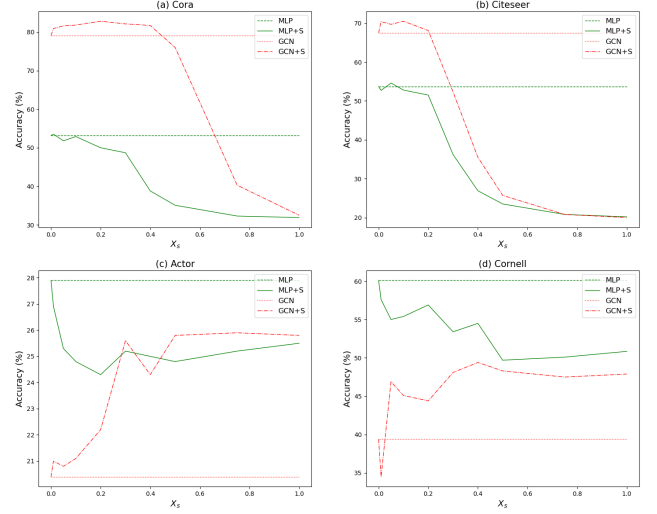


Figure 8: Variation of node classification accuracy w.r.t. the shifted value X_s on four benchmark datasets

Table 4: Node classification accuracy (%) on six benchmark datasets. We describe X_s with the best performance

Methods	MLP	MLP+S	X_s	GCN	GCN+S	X_s
Cora	53.2	53.5	0.01	79.1	82.8	0.2
Citeseer	53.7	54.6	0.05	67.5	70.5	0.1
Actor	27.9	27.9	0	20.4	25.9	0.9
Cornell	60.1	60.1	0	39.4	49.4	0.5
Texas	65.8	71.4	0.2	47.6	53.0	0.1
Wisconsin	73.5	73.5	0	40.5	50.2	0.1

B ANALYSIS OF SHIFTING FEATURES

In Equation 8, we suggest that shifting can be one solution to solve the gradient vanishing problem. Specifically, adding a small value X_s to the initial feature X can remove the zero elements as below:

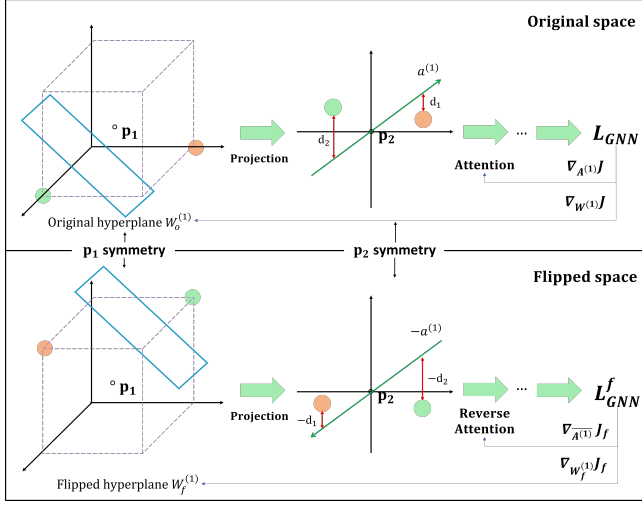
$$X = X + X_s.$$

In Figure 8 and Table 4, we measure node classification accuracy of two baselines (MLP, GCN) using original inputs X and their another version (MLP+S, GCN+S) with shifted inputs $X + X_s$. We didn't renormalize $X + X_s$ here. The symbol (+S) means shifting is applied to a baseline model. Here, three datasets (Pubmed, Chameleon, Squirrel) are excluded since they contain a majority of non-zero elements. The X_s of each dataset is selected through a grid search that shows the best validation score.

In Figure 8, we can see that shifting for GCN has a greater impact, where the performance has improved for all datasets. Conversely, shifting for MLP generally downgrades the overall quality except for one dataset (Texas). We think that as the number of non-zero elements increases, a model requires more training samples. Since MLP only utilizes a central node compared to GNNs, shifting itself fails to guide the multiple parameters precisely.

Table 5: Node classification accuracy (%) w.r.t. the different number of training samples

Dataset	Pubmed			Actor			Chameleon			Squirrel			Cornell			Texas			Wisconsin		
	L/C	20	40	80	20	40	80	20	40	80	20	40	80	5	10	20	5	10	20	5	10
z-value	0.96	1	1	0.21	0.34	0.5	1	1	1	1	1	1	0.62	0.72	0.84	0.41	0.63	0.78	0.53	0.71	0.85
MLP	69.7	71.3	71.8	27.9	29.0	30.1	41.2	46.3	49.1	26.5	28.7	29.7	60.1	68.8	73.3	65.8	71.4	75.6	73.5	77.0	79.5
MLP+F	74.1	75.9	77.1	35.9	37.4	38.2	43.5	49.9	51.8	28.5	30.9	31.8	70.5	86.4	95.8	79.2	83.3	94.3	80.5	84.2	88.9
GCN	77.8	78.6	79.1	20.4	20.7	21.1	49.4	53.5	55.7	31.8	35.5	37.6	39.4	50.7	53.3	47.6	52.7	54.7	40.5	43.5	46.1
GCN+F	79.2	81.3	82.1	28.6	29.9	30.7	50.4	53.7	55.7	32.4	36.3	37.7	52.4	54.9	72.8	62.2	65.8	78.6	52.3	52.9	60.5
GAT	78.0	80.1	80.8	22.5	23.1	23.5	46.9	52.4	54.1	30.8	32.4	33.3	42.1	48.9	53.3	49.2	51.4	56.3	45.8	46.0	47.6
GAT+F	78.8	81.0	82.2	30.3	30.6	30.7	48.3	49.6	53.0	31.9	32.8	33.4	50.6	59.5	64.4	61.0	67.1	76.3	54.5	58.7	64.8

**Figure 9: The overview of the first layer in Flip-GAT. Compared to Flip-GCN, they further employ attention layer $a^{(1)}$ whose value is origin symmetry**

C MORE EXPERIMENTAL RESULTS OF RQ3

In addition to Table 3, we also measure the performance of another seven datasets by varying the number of labeled nodes. The results can be seen in Table 5. Further, we describe the z-value of central nodes that are defined in Equation 1 concerning the labeled node per class (L/C). Since the WebKB dataset is a relatively small graph, the L/C is set to $\{5, 10, 20\}$. The methods with a symbol (+F) mean that a flip is applied. Here, we can see that the methods with flipping significantly outperform the baselines. However, in some cases like Chameleon and Squirrel, integrating flip merely improves the overall quality of plane GNNs. Remember that all elements of the initial features of these datasets are non-zero (z-value is 1) and their maximal values are high. Thus, as the labeled node increases, the vanilla GCN shows good performance since a first hyperplane might generalize well without flipping. This also happens to GAT, where the performance gap between GAT and GAT+F becomes smaller as L/C rises. But in another dataset, the flipping introduces a significant gain. For example, in three WebKB graphs (Cornell, Texas, Wisconsin), the accuracy of all methods grows almost exponentially w.r.t. the L/C samples. Throughout these results, we contemplate that integrating a flipping can secure robustness and generalize to certain kinds of features.

D DETAILS OF FLIP-GAT

Since Flip-MLP is a simple modification of Flip-GCN that removes an adjacency matrix, we do not treat them precisely. In Figure 9, we show the overall architecture of Flip-GAT. Since GAT employs an attention layer which is defined in Equation 4, we should consider this for both spaces. Firstly, we discuss the forward propagation in an original space as below:

$$A_{ij}^{(l)} = \frac{\exp(\sigma(a^{(l)}[h_i^{(l)}||h_j^{(l)}]))}{\sum_{k \in N_i} \exp(\sigma(a^{(l)}[h_i^{(l)}||h_k^{(l)}]))}, \quad (l \geq 1)$$

$$H^{(l+1)} = \sigma(\bar{H}^{(l+1)}), \quad \bar{H}^{(l+1)} = A^{(l)} H^{(l)} W_o^{(l)}$$

$$\hat{Y} = \text{softmax}(\bar{H}^{(L)}).$$

During backpropagation, the gradients of W that is considered a multi-head projection matrix are defined as follows:

$$\nabla_{W^{(l)}} J = (A^{(l)} H^{(l)})^T \nabla_{\bar{H}^{(l+1)}} J, \quad (l \geq 1).$$

Also, referring to Eq. 6, we can retrieve the gradients of the attention layer as below:

$$\nabla_{A^{(l)}} J = (H^{(l)} W^{(l)})^T \nabla_{\bar{H}^{(l+1)}} J, \quad (l \geq 1).$$

In a flipped space, the forward propagation is quite similar to Eq. 12 but we should multiply the negative constant (-1) by the first layer attention vector. As described in the middle of Figure 9, the attention values d_1, d_2 are p_2 (origin) symmetry. Thus, the forward propagation is defined as follows:

$$\bar{A}_{ij}^{(1)} = \frac{\exp(\sigma(-a^{(1)}[h_i^{(1)}||h_j^{(1)}]))}{\sum_{k \in N_i} \exp(\sigma(-a^{(1)}[h_i^{(1)}||h_k^{(1)}]))}$$

$$H_f^{(2)} = -\sigma(\bar{A}^{(1)} X_f W_f^{(1)}), \quad (l = 1)$$

$$H_f^{(l+1)} = \sigma(\bar{H}_f^{(l+1)}), \quad \bar{H}_f^{(l+1)} = A^{(l)} H_f^{(l)} W_f^{(l)}, \quad (l \geq 2)$$

Likewise, the gradients of W are as follows:

$$\nabla_{W_f^{(1)}} J_f = (\bar{A}^{(1)} X_f)^T \nabla_{\bar{H}_f^{(2)}} J_f, \quad \bar{H}_f^{(2)} = \bar{A}^{(1)} X_f W_f^{(1)}, \quad (l = 1)$$

$$\nabla_{W_f^{(l)}} J_f = (A^{(l)} H_f^{(l)})^T \nabla_{\bar{H}_f^{(l+1)}} J_f, \quad (l \geq 2).$$

Similarly, the attention vectors are updated as below:

$$\nabla_{\bar{A}^{(1)}} J_f = -(H_f^{(1)} W_f^{(1)})^T \nabla_{\bar{H}_f^{(2)}} J_f, \quad (l = 1)$$

$$\nabla_{A^{(l)}} J_f = (H_f^{(l)} W_f^{(l)})^T \nabla_{\bar{H}_f^{(l+1)}} J_f, \quad (l \geq 2).$$